AMERICAN SOCIETY FOR MICROBIOLOGY | Journal of Bacteriology®

RESEARCH ARTICLE

Conformational Changes of an Interdomain Linker Mediate Mechanical Signal Transmission in Sensor Kinase BvgS

Elodie Lesne, Elian Dupré,* Camille Locht, Rudy Antoine, Françoise Jacob-Dubuisson

Université Lille, CNRS, INSERM, CHU Lille, Institut Pasteur de Lille, U1019-UMR 8204-CIIL, Centre d'Infection et d'Immunité de Lille, Lille, France

ABSTRACT The whooping cough agent, *Bordetella pertussis*, controls the expression of its large virulence regulon in a coordinated manner through the two-component system BvgAS. BvgS is a dimeric, multidomain sensor kinase. Each monomer comprises, in succession, tandem periplasmic Venus flytrap (VFT) domains, a transmembrane segment, a cytoplasmic Per-Arnt-Sim (PAS) domain, a kinase module, and additional phosphorelay domains. BvgS shifts between kinase and phosphatase modes of activity in response to chemical modulators that modify the clamshell motions of the VFT domains. We have shown previously that this regulation involves a shift between distinct states of conformation and dynamics of the two-helix coiled-coil linker preceding the enzymatic module. In this work, we determined the mechanism of signal transduction across the membrane via a first linker, which connects the VFT and PAS domains of BvgS, using extensive cysteine cross-linking analyses and other approaches. Modulator perception by the periplasmic domains appears to trigger a small, symmetrical motion of the transmembrane segments toward the periplasm, causing rearrangements of the noncanonical cytoplasmic coiled coil that follows. As a consequence, the interface of the PAS domains is modified, which affects the second linker and eventually causes the shift of enzymatic activity. The major features of this first linker are well conserved among BvgS homologs, indicating that the mechanism of signal transduction unveiled here is likely to be generally relevant for this family of sensor kinases.

IMPORTANCE *Bordetella pertussis* produces virulence factors coordinately regulated by the two-component system BvgAS. BvgS is a sensor kinase, and BvgA is a response regulator that activates gene transcription when phosphorylated by BvgS. Sensor kinases homologous to BvgS are also found in other pathogens. Our goal is to decipher the mechanisms of BvgS signaling, since these sensor kinases may represent new targets for antibacterial agents. Signal perception by the sensor domains of BvgS triggers small motions of the helical linker region underneath. The protein domain that follows this linker undergoes a large conformational change that amplifies the initial signal, causing a shift of activity from kinase to phosphatase. Because BvgS homologs harbor similar regions, these signaling mechanisms are likely to apply generally to that family of sensor kinases.

KEYWORDS *Bordetella pertussis*, PAS domain, coiled coil, sensory transduction processes, two-component regulatory systems, virulence regulation

Received 20 February 2017 **Accepted** 8 May 2017

Accepted manuscript posted online 15 May 2017

Citation Lesne E, Dupré E, Locht C, Antoine R, Jacob-Dubuisson F. 2017. Conformational changes of an interdomain linker mediate mechanical signal transmission in sensor kinase BvgS. J Bacteriol 199:e00114-17. https://doi.org/10.1128/JB.00114-17.

Editor Ann M. Stock, Rutgers University-Robert Wood Johnson Medical School

Address correspondence to Rudy Antoine, rudy.antoine@pasteur-lille.fr, or Françoise Jacob-Dubuisson, francoise.jacob@ibl.cnrs.fr.

* Present address: Elian Dupré, University of Lille, CNRS, UMR 8576, UGSF, Villeneuve d'Ascq, France.

Two-component systems (TCS) are widely used by eubacteria for adaptation to environmental stimuli (1, 2). Canonical TCS are composed of a transmembrane sensor kinase and a response regulator protein. Following the perception of a specific

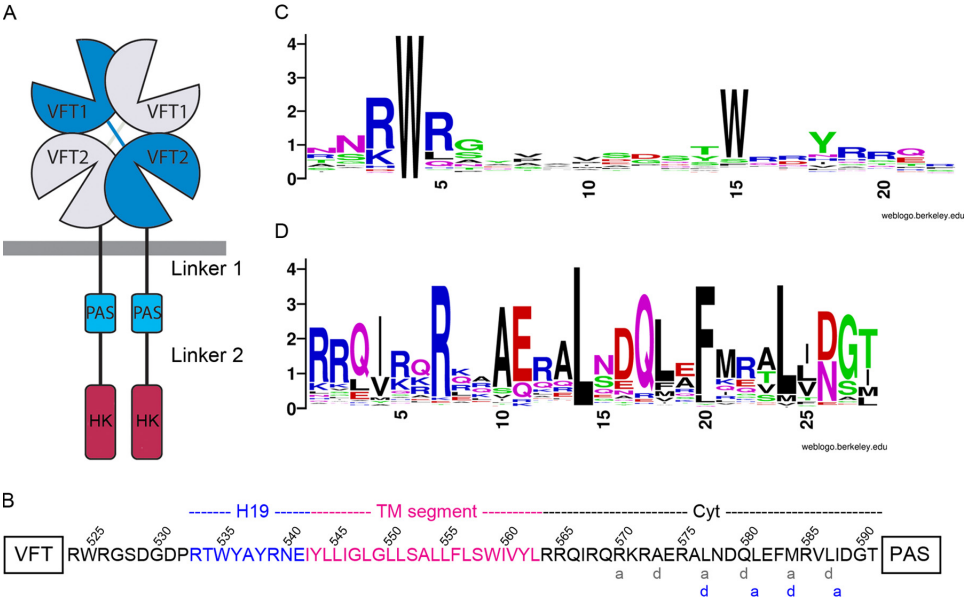

FIG 1 The VFT-PAS linker of BvgS. (A) Schematic representation of the BvgS dimer. The VFT, PAS, and histidine kinase (HK) domains are represented, but the receiver and HPt domains have been omitted for clarity. The VFT-PAS and PAS-HK linkers are designated linker 1 and linker 2, respectively. (B) Amino acid sequence of linker 1, showing the "a" and "d" positions of the two coiled-coil registers predicted for this segment (gray and blue letters below the sequence). (C and D) WebLogo representations of the consensus sequences for the H19 helices (C) and the cytoplasmic portion of linker 1 (D) based on sequence alignments of BvgS homologs harboring two VFT domains and one PAS domain.

signal by the sensor kinase, the kinase domain autophosphorylates and transfers the phosphoryl group to the response regulator, triggering its activation and allowing specific adaptive responses (3, 4). Unorthodox systems contain additional domains involved in a phosphorelay, which provides checkpoints to regulate the activity of the sensor kinase (5).

The whooping cough agent, *Bordetella pertussis*, produces a number of virulence factors to colonize the human respiratory tract. The expression of the virulence regulon is controlled by a TCS called BvgAS. BvgA is a classical response regulator, which, when phosphorylated, acts as a transcriptional activator of the virulence regulon, thus placing the bacteria in the Bvg^+, virulent phase (6). BvgS is a dimeric sensor kinase. Each monomer is composed of two tandem periplasmic Venus flytrap (VFT) domains (Pfam SBP_bac_3), a transmembrane (TM) segment, a cytoplasmic Per-Arnt-Sim (PAS) domain, and a histidine kinase (HK) moiety of the HisK-A type according to the Pfam nomenclature, comprising a dimerization and histidine phosphotransfer (DHp) domain and a catalytic ATP-binding (CA) domain (Fig. 1A) (7). These domains are followed by a receiver and a histidine phosphotransfer (HPt) domain, which form a phosphorelay (8).

BvgS is in a kinase mode of activity by default, i.e., at 37°C, under standard culture conditions, and without the perception of a specific activating ligand. In the laboratory, the bacteria shift to the avirulent Bvg^- phase in response to the perception by BvgS of modulators such as $MgSO_4$ or nicotinate, at low temperatures, or under conditions of nutrient restriction (9–12). We have shown, using a Phos-tag assay, that addition of nicotinate to the bacteria causes the dephosphorylation of BvgA much faster than if the reaction occurs spontaneously (12). This indicates that BvgS switches to the phosphatase mode of activity under those conditions. In the default state of BvgS, the kinase activity of the protein depends on the dynamics of its membrane-distal "VFT1" domains (7). At the molecular level, we have shown that the binding of nicotinate or related molecules to the membrane-proximal "VFT2" domains of BvgS rigidifies the entire periplasmic moiety and decreases its dynamics (12, 13). These modifications of the VFT domains induce conformational changes to the cytoplasmic portion of BvgS that cause the shift toward phosphatase activity.

In BvgS, long segments predicted to be α-helical, and referred to below as "linker 1" and "linker 2," connect the VFT to the PAS domains and the PAS to the DHp domains of the kinase moiety, respectively (14, 15) (Fig. 1A). Both linkers are highly conserved among *B. pertussis* isolates, and they have been proposed to perform mechanical signal transduction (14). In the dimer, linker 1 and linker 2 are predicted to form coiled coils. Canonical two-helix coiled coils are generally left-handed, and their parallel α-helices are characterized by heptads of amino acid residues that form two helical turns, denoted by the letters "abcdefg" (16–18). The "a" and "d" residues at the central positions of the coiled coil are generally hydrophobic and nonaromatic. The other residues of the helix are rather polar and favor helix formation. The stability of the coiled coil depends on both ionic and hydrophobic interactions (17, 19–21). A recent study has demonstrated that unlike structural coiled coils, signaling coiled coils harbor irregularities that enable them to switch between distinct, energetically stable conformations (18).

PAS domains are ubiquitous and are involved in sensory and regulatory functions (22–24). They are defined by a structural motif that consists of a five-stranded antiparallel β-sheet flanked on one side by α-helices. The β-sheet is often involved in dimerization, and changes in the quaternary structure of the PAS domains, i.e., dissociation, dimerization, rotation, or scissor movement of one monomer relative to the other, are involved in signal transduction (22, 23, 25–27). Our earlier studies have indicated the remarkable conservation of the BvgS PAS domain among *Bordetella* isolates and have shown the importance of the PAS core fold for the regulation of BvgS activity (14, 28). We have proposed that the PAS domain serves as a toggle switch (29).

The activity of BvgS is determined by the balance between rigidity and dynamics in linker 2, located between the PAS and the HK domains. The kinase mode is characterized by considerable rotational dynamics in this region, whereas in the phosphatase mode, linker 2 adopts its stable, hydrophobic coiled-coil interface (29). The manner in which the dynamics of VFT domains are transmitted to linker 2, and in particular the mechanism by which the intervening linker 1 and PAS domains of BvgS mediate this signaling, is the focus of this work. We determined the topology of linker 1 in the kinase and phosphatase modes. We found out that modulator perception by the VFT domains causes small conformational changes in linker 1, leading to a change in the PAS domain interface that triggers the activity shift of BvgS.

RESULTS

Organization and conservation of the VFT-PAS linker. Linker 1, located between the VFT2 and PAS domains of each monomer, is composed, successively, of a periplasmic α-helix called H19, a hydrophobic region harboring a TM segment, and a mostly hydrophilic cytoplasmic α-helix (Fig. 1B). We collected the nonredundant sequences of 562 BvgS homologs, comprising two VFT domains and one PAS domain, to analyze the features of linker 1 in the family. The sequence of H19 is not conserved, except for a Trp residue (W_{535} in BvgS), located in most sequences 11 residues after that of the conserved Arg-Trp-Arg motif ($R_{524}W_{525}R_{526}$ in BvgS) of the last α-helix of most VFT2 domains (Fig. 1C; see also Fig. S1 in the supplemental material). Sequence alignments show that in a few family members, the Trp residue in H19 is found 10 residues—as in BvgS—or 12 residues after the RWR motif of VFT2 (Fig. S1). The sequence of the following hydrophobic segment is predicted to correspond to a 22-residue TM domain (Fig. 1B; see also Fig. S2 in the supplemental material). The cytoplasmic portion of linker 1 comprises 28 residues in BvgS, some of which are almost invariant in the family (Fig. 1D; see also Fig. S3 in the supplemental material). Although this length appears to be most common, the cytoplasmic segment is a few residues shorter or longer in some family members (Fig. S3). In BvgS, this region is predicted to form a heptad-based coiled coil, with two possible, partially overlapping registers (Fig. 1B, gray and blue letters). The residues at the interface "a" and "d" positions are rather well conserved, including some hydrophilic residues (Fig. 1D).

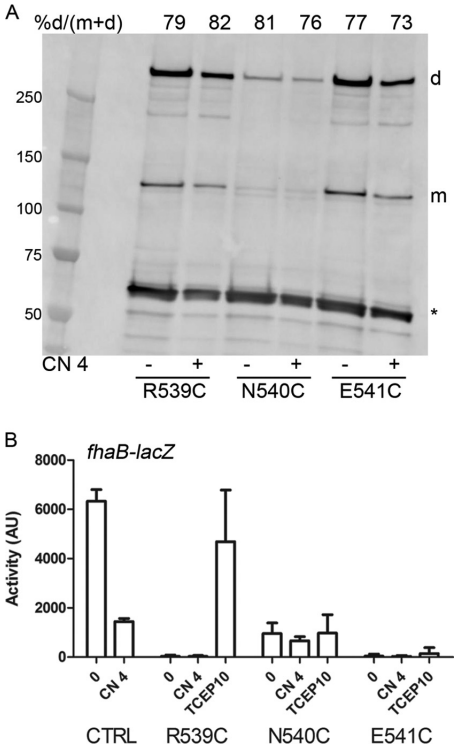

FIG 2 Topology of the C-terminal periplasmic residues of linker 1. (A) Spontaneous intermomoner S-S bond formation in *B. pertussis* grown under basal conditions (−) or after the addition (+) of 4 mM chloronicotinate (CN 4). No oxidative treatment was applied in these experiments, in contrast to those performed with *E. coli* (see Fig. 3, 6, and 7). BvgS^{fl} was detected with anti-BvgS antibodies. m, monomeric form; d, dimeric form. Dimer proportions are given at the top of each lane. The loading control is an unidentified *B. pertussis* protein fortuitously recognized by the antibodies (indicated by an asterisk). (B) The *fhaB-lacZ* reporter was used to determine the activities of the BvgS^{fl} variants under basal conditions (0) or after the addition of 4 mM chloronicotinate or 10 mM tris(2-carboxyethyl)phosphine (TCEP; added as a reducing agent 6 h before the culture was harvested). All variants harbor the $C_{607}A$ and $C_{881}S$ substitutions as in the control (CTRL), which corresponds to the strain producing BvgS^{fl}. Data shown are means and standard errors of the means.

Interestingly, canonical parallel two-helix coiled coils are overwhelmingly left-handed (18, 30, 31). In contrast, the X-ray structure of the periplasmic moiety of BvgS shows that the two BvgS monomers coil around each other in a right-handed twist (7). This mismatch needs to be accommodated in the long predicted helix formed by linker 1.

Importance of the membrane-proximal periplasmic residues of linker 1. The X-ray structure of the periplasmic moiety of BvgS shows that the H19 helices splay out, each forming interactions with the second lobe of the opposite monomer (7). In particular, W_{535} is buried in a strongly hydrophobic and aromatic pocket, where it forms several pi interactions and van der Waals contacts with surrounding residues. The replacement of W_{535} with Ala abrogates BvgS activity, indicating the importance of the H19–VFT2 connection for BvgS function (7). We replaced residues R_{539}, N_{540}, and E_{541}, further into H19, with Cys to determine the topology and dynamics of the membrane-proximal periplasmic residues. Thus, we measured the proportions of spontaneous *in vivo* intermonomer disulfide (S-S) bond-mediated cross-linking in bacteria grown under default (i.e., kinase-promoting) or modulating (i.e., phosphatase-promoting) conditions. These substitutions were introduced into a full-length version of BvgS called BvgS^{fl}, in which two naturally occurring Cys_{607} and Cys_{881} residues were replaced by Ala and Ser, respectively (29). Remarkably, high proportions of S-S cross-linking were detected at all three positions, with dimer-to-monomer ratios of approximately 70% under both growth conditions (Fig. 2A). The effects of these substitutions on BvgS activity were determined in *B. pertussis* by measuring the β-galactosidase (β-Gal) activities of *ptx-lacZ*

and *fhaB-lacZ* transcriptional fusions. Both systems report BvgS kinase activity, but *ptx-lacZ* expression and *fhaB-lacZ* expression require high and low proportions of phosphorylated BvgA, respectively (32). The *fhaB-lacZ* fusion is thus used to measure intermediate levels of activity barely detectable with the other reporter. The phosphatase state corresponds to low or no activity with either reporter. Even with the *fhaB-lacZ* reporter, the three BvgS Cys variants showed little or no kinase activity at the basal state or after modulation, suggesting that they are locked in the phosphatase state (Fig. 2B). However, the $BvgS^{fl}_{N540C}$ variant was detected at low steady-state levels in cell extracts, indicating a biogenesis defect or increased sensitivity to proteolysis (Fig. 2A). Treatment of the cultures with reducing agents restored the kinase activity of the $BvgS_{R539C}$ variant, but for the other two variants, it did not markedly decrease S-S bond formation, and no activity was recovered (Fig. 2B; see also Fig. S4A in the supplemental material). Substitution of N_{540} and E_{541} with Ala yielded active and inactive variants, respectively, but even the inactive variant was produced at normal levels (Fig. S4B to D). Therefore, the Glu_{541} residue appears to be essential for BvgS function, while in the other two cases, the presence of the S-S bond, rather than the replacement of the initial residues, is the most likely reason for the loss of activity. Strong spontaneous intermonomer S-S bond-mediated cross-linking at four successive positions (positions 539 to 542; see below for Ile_{542}Cys) suggests that the α-helix conformation is disrupted in that region and that this segment is very dynamic. The short R_{539}-N_{540}-E_{541} segment is thus probably extended in a cable-like conformation with very close intermonomer contacts. Tying these short segments to each other in a symmetric manner freezes BvgS in the phosphatase mode.

Topology and response to modulation of the transmembrane segment. To determine the organization of the hydrophobic segment of linker 1, Cys-scanning S-S cross-linking analyses were performed in *Escherichia coli* using a truncated BvgS variant called $BvgS^{t}$. $BvgS^{t}$ is devoid of the receiver and HPt domains, and it harbors mutations of its natural Cys residues as described above, as well as a C-terminal 6-His tag for immune detection (29). The corresponding $BvgS^{fl}$ variants were also constructed to determine BvgS activity in *B. pertussis*. Residues 542 to 561 were individually replaced with Cys in $BvgS^{t}$ and $BvgS^{fl}$. Intermonomer S-S bond formation was determined after oxidative treatment of the bacteria with copper-*o*-phenanthroline (Cu-oP) and immunodetection of $BvgS^{t}$ in membrane extracts under nonreducing conditions.

In the first part of this segment, comprising residues I_{542} to G_{549}, S-S bonds were detected in a periodic manner, suggesting proximity of the two TM α-helices with some rotational dynamics, consistent with a fluid membrane environment (Fig. 3A and B). In the central part of the hydrophobic segment (residues 550 to 554), low proportions of S-S bonds were observed, suggesting that the helices are more distant from one another, or that the oxidizing agent could not reach the central part of the lipid bilayer. In the last part of the predicted segment, comprising residues L_{555} to V_{561}, S-S bonds were again detected in a periodic manner.

Modulation of the cultures did not modify the S-S bond patterns for residues 542 to 549 or residues 554 to 561 and caused only slightly increased cross-linking in the intervening segment (residues 550 to 553) (Fig. 3A and B). The similar cross-linking patterns under the two conditions argue that the two helices do not appear to move relative to one another in response to modulation. One should keep in mind, however, that the membrane allows high α-helix dynamics, and therefore, some motions might be missed by the Cys-scanning technique (33).

By and large, the corresponding $BvgS^{fl}$ Cys variants displayed kinase activity and were sensitive to modulation (Fig. 3C and D). However, the replacement of Gly_{547}, Trp_{559}, and Ile_{560} with Cys considerably affected BvgS kinase activity, and that of Gly_{549} led to insensitivity to modulation. These low-activity variants were properly produced in *B. pertussis*, and no spontaneous S-S cross-linking was detected in either case (see Fig. S5A in the supplemental material).

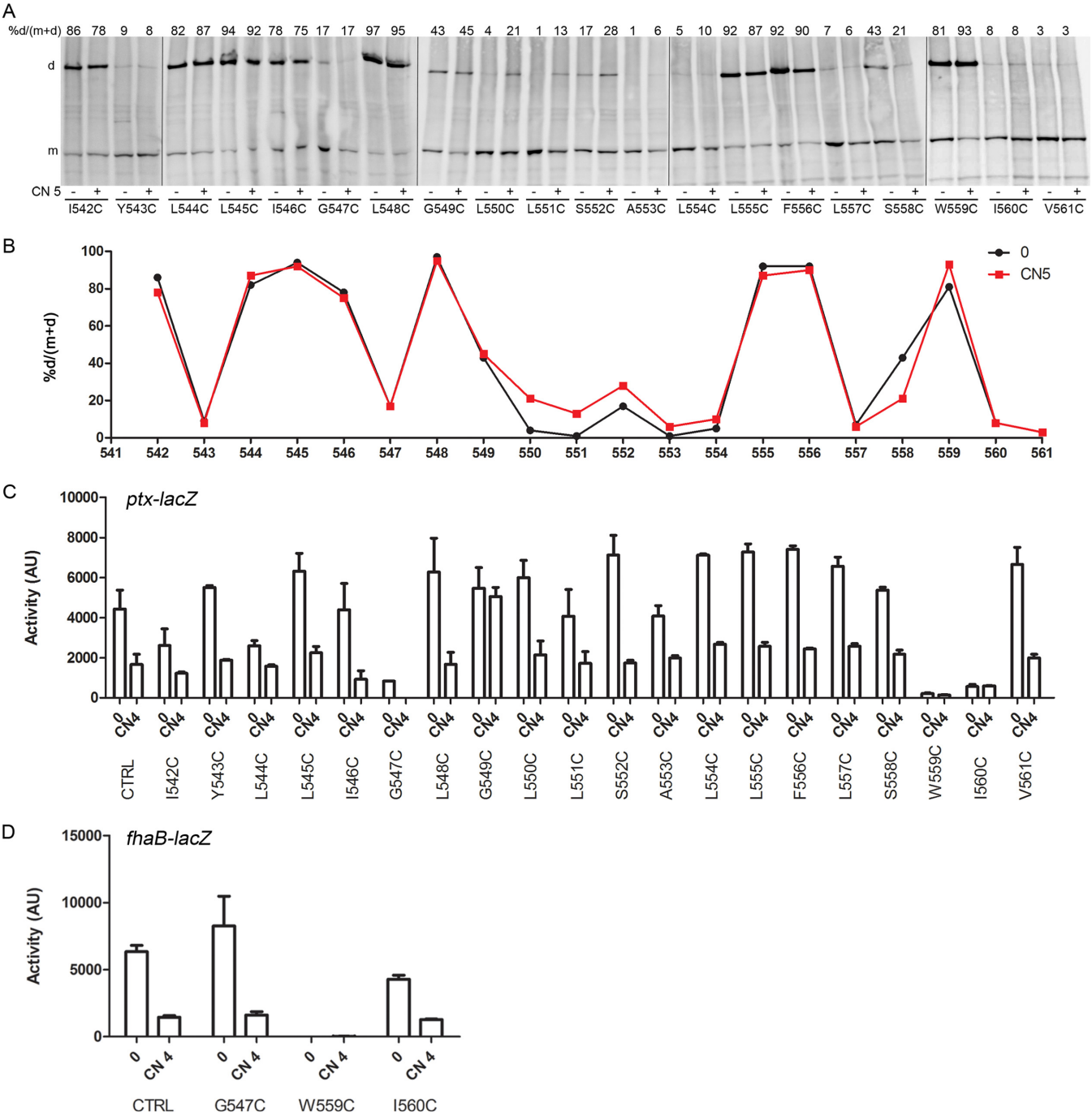

FIG 3 Topology of the transmembrane segment. (A) Cys-scanning analyses for the BvgS^t variants were performed in *E. coli* under basal conditions (−) or after the addition (+) of 5 mM chloronicotinate (CN 5). An oxidative treatment was performed to enhance intradimer S-S bond formation. BvgS^t was detected using anti-His tag antibodies. m and d, monomeric and dimeric forms, respectively. Dimer proportions are given at the top of each lane. (B) The results of a representative experiment were graphed to facilitate reading. Dimer proportions are shown under basal conditions (0) and after the perception of chloronicotinate (CN 5). (C and D) The activities of the BvgS^{fl} variants were determined in *B. pertussis* using the *ptx-lacZ* (C) or *fha-lacZ* (D) reporter under basal conditions (0) or after the perception of 4 mM chloronicotinate (CN 4). Data shown are means and standard errors of the means. All variants also harbor the $C_{607}A$ and $C_{881}S$ substitutions, as in the control (CTRL).

Thus, the relative positions of the two TM helices are little modified upon the kinase-to-phosphatase shift. This argues against large displacement of the two helices relative to one another in response to modulation. Interestingly, similar results have been reported for the sensor kinases DcuS and EnvZ (34, 35). Those authors have instead proposed a symmetrical piston movement of the TM helices to transduce the

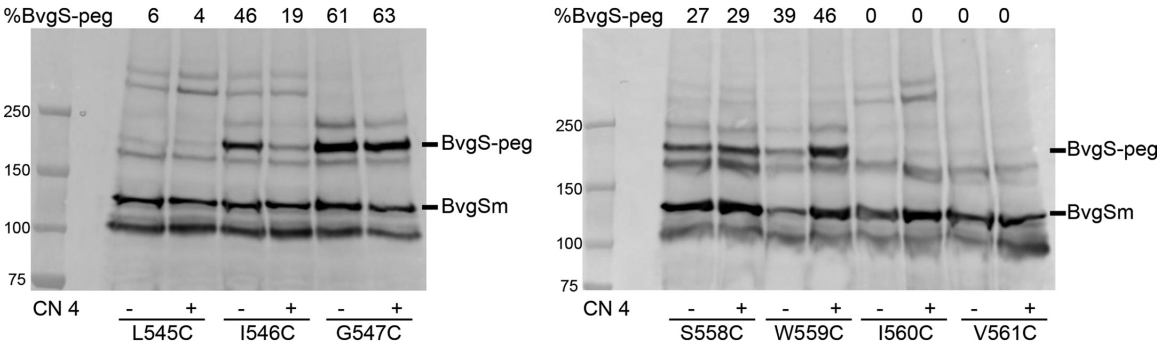

FIG 4 Conformational change of the transmembrane segment in response to modulation. Cys accessibility experiments were performed in *B. pertussis* on BvgS^{fl} variants under basal (−) or modulated (chloronicotinate [CN] added to 4 mM) (+) growth conditions. Monomeric BvgS (BvgSm) and BvgS modified by PEG-maleimide (BvgS-peg) are indicated. The proportions of the PEG-modified form are given at the top of each lane.

signal. To test this hypothesis with BvgS, we performed Cys accessibility experiments in *B. pertussis* in order to distinguish between residues outside and inside the hydrophobic portion of the lipid bilayer (34). Briefly, the bacteria were treated with *N*-ethylmaleimide (NEM) to modify the free Cys residues that are in a hydrated environment on either side of the membrane. NEM can cross lipid bilayers, but it can modify sulfhydryl groups only in the presence of water molecules. After bacterial lysis and membrane permeabilization, treatment with polyethylene glycol (PEG)-maleimide (Peg-Mal; molecular mass of 20 kDa) was used to label Cys residues previously protected from NEM by the hydrophobic environment. The binding of Peg-Mal to BvgS was detected by immunoblot analyses, since it causes an electrophoretic mobility shift.

These experiments were performed with BvgS^{fl} harboring one Cys residue at a time from position 543 to 550 at the periplasmic end of the TM segment and from position 558 to 565 at the other end. BvgS$^{fl}_{Cys543}$ to BvgS$^{fl}_{Cys545}$ were not modified by Peg-Mal (i.e., these Cys residues were blocked by NEM) when the bacteria were grown under either basal or modulating conditions (Fig. 4; see also Fig. S6 in the supplemental material), indicating that they are in a partially hydrated environment. In contrast, Peg-Mal binding to BvgS$^{fl}_{Cys546}$ under basal growth conditions showed that the residue is in the fully dehydrated portion of the membrane (Fig. 4). However, the addition of a modulator caused a marked decrease in the intensity of the Peg-Mal-labeled band of BvgS$^{fl}_{Cys546}$. The Cys residues after position 546 were modified by Peg-Mal under both conditions, showing that they are in the hydrophobic layer of the membrane (Fig. 4; also Fig. S6). In the C-terminal portion of the TM segment, the Cys residues at positions 558 and 559 were modified by Peg-Mal, while those at positions 560 to 565 were not (i.e., their Cys residues were blocked by NEM). Thus, these data indicate that the latter six Cys residues are not in a fully dehydrated environment but most likely at the interface of the apolar and polar regions of the membrane (Fig. 4; also Fig. S6). After modulator addition, a slight increase in the level of Peg-Mal labeling was observed at position 559, which seems to mirror the effect at position 546. These results are qualitatively consistent with the model that the response to modulation implies a small, symmetrical movement of the TM helices toward the periplasm, in a manner similar to that observed in the sensor kinase DcuS, but with a smaller amplitude (34). However, additional movements of the TM helices cannot be ruled out with the current data.

Cytoplasmic portion of linker 1: topology and role in BvgS regulation. The cytoplasmic portion of linker 1 is predicted to form a noncanonical coiled coil, with two possible registers that partially overlap (Fig. 1B). Its sequence is rather well conserved in the family (Fig. 1D; also Fig. S3 in the supplemental material). However, some family members have linker lengths different from that of BvgS (Fig. S3). To probe the link between length and function, we replaced this 28-residue region of BvgS with very similar sequences of homologs that are 1 residue shorter or 1, 2, or 3 residues longer (see Fig. S7A in the supplemental material). All the resulting variants were inactive (Fig.

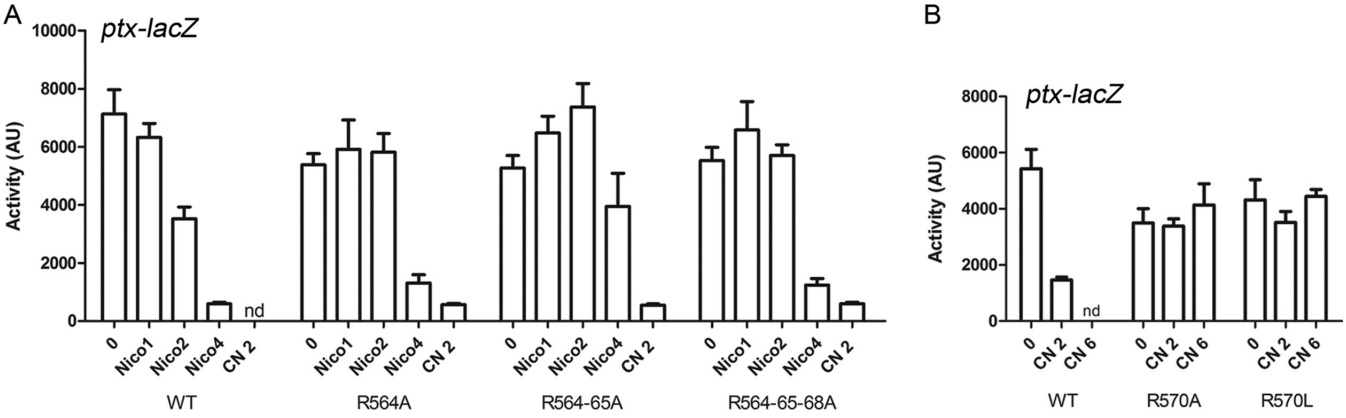

FIG 5 Roles of membrane-proximal charged residues in BvgS regulation. (A and B) The *ptx-lacZ* reporter was used to determine the activities of the BvgS variants compared to that of the wt strain at the basal state or after the addition of increasing millimolar concentrations of modulators (nicotinate [Nico] and chloronicotinate [CN]). Data shown are means and standard errors of the means. nd, not determined.

S7B). However, they were produced at high levels, indicating no biogenesis defect and no increased sensitivity to proteolysis (Fig. S7C).

Interestingly, the composition of the first segment of the cytoplasmic part of linker 1 is strongly biased toward positively charged residues, in particular Arg, and this feature is conserved in the family (Fig. 1D; also Fig. S3 in the supplemental material). We targeted the first four Arg residues to determine their role in BvgS regulation. The progressive replacement of R_{564}, R_{565}, and R_{568} with Ala slightly decreased the response of BvgS to intermediate concentrations of nicotinate (Fig. 5A), and the replacement of R_{570} with Ala or Leu yielded totally insensitive variants (Fig. 5B). Thus, the positive charges in this region participate in signal transduction. Of note, Arg_{570}, which is in the "a" position of the putative coiled coil, is almost invariant in the family (Fig. 1D).

Next, we performed Cys scanning S-S cross-linking analyses on the N-terminal (Y_{562}-to-I_{567}) and C-terminal (L_{577}-to-I_{588}) segments of the cytoplasmic portion of the linker 1 region to probe their topologies and their responses to modulation. The analyses indicated close contacts between helices, with high proportions of cross-links at predicted "a" and "d" coiled-coil positions (Fig. 6A and B). In the C-terminal segment, high proportions of S-S bonds were observed at positions 577, 581, 584, and 588, indicating that the second coiled-coil register is favored (Fig. 6B, blue letters). Note that the cross-linking pattern obtained might also be consistent with a hendecad-based, 11-residue coiled coil, with apolar and rather well conserved residues at the "a," "d," "e," and "h" positions (36) (Fig. 6B, green letters). However, the cross-linking results at positions 563, 580, and 588 must be discarded, since the corresponding Cys substitutions abolished BvgS activity (see below).

Interestingly, the addition of a modulator markedly decreased the proportions of intermonomer S-S bonds at most positions in the segment comprising residues 581 to 587. Globally, the periodic pattern of cross-linking detected in that segment in the kinase state was interrupted in the phosphatase state. This suggests that a change in coiled-coil packing took place or that the α-helices splayed apart in this segment.

The activities of the corresponding $BvgS^{fl}$ Cys variants and of additional $BvgS^{fl}$ variants with Ala or Leu substitutions were determined using the reporter systems. They revealed altered phenotypes for the replacement of some conserved residues (Fig. 6C and D). In particular, replacement of L_{563} with Cys abrogated BvgS activity, as did replacement of Q_{580} with Cys or Leu and replacement of I_{588} with Cys (Fig. 6D; see also Fig. S8A and B in the supplemental material). The observations that the inactive $BvgS^{fl}$ variants were produced at normal levels in *B. pertussis* and that the level of spontaneous intermonomer S-S bond formation was low (Fig. S5B and S8C) indicated that the residues at positions 563, 580, and 588 are essential for BvgS function. In addition, single substitutions of L_{577}, D_{579}, F_{583}, and R_{585} with Cys, of M_{584} with Leu, and of L_{587}

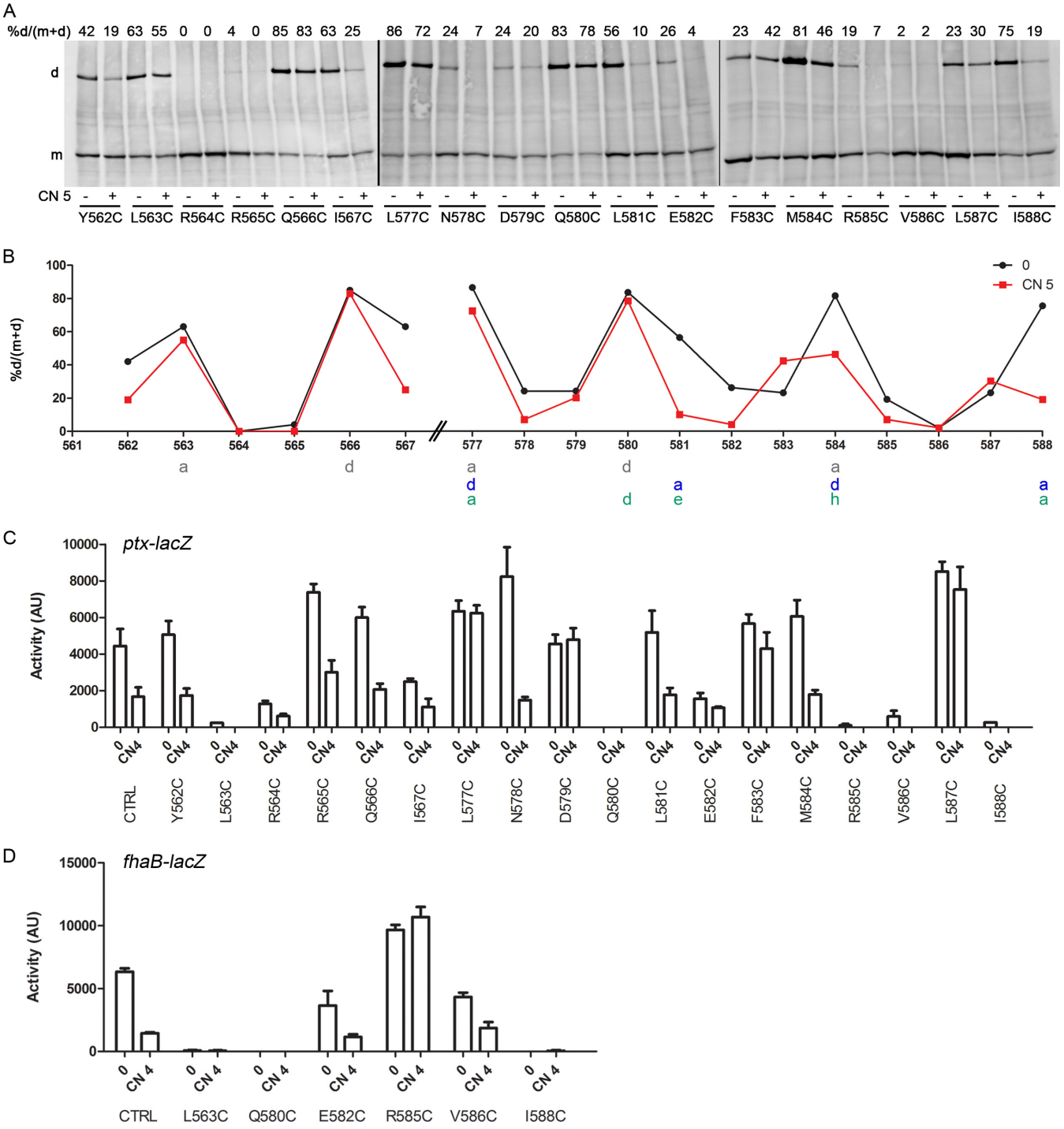

FIG 6 Topology of the cytoplasmic portion of linker 1. (A) Cys-scanning analyses of the BvgS^{t} variants were performed under basal conditions (−) or after the addition of 5 mM chloronicotinate (CN 5) (+). Experimental details are the same as those for Fig. 3. (B) The results of a representative experiment were graphed to facilitate reading. The "a" and "d" positions of the two heptad-based coiled-coil predictions are indicated below the graph in gray and blue letters. The periodicity of a potential hendecad-based coiled coil is indicated in green letters. Dimer proportions are shown under basal conditions (0) or after the addition of 5 mM chloronicotinate (CN 5). (C and D) The activities of the BvgS^{fl} variants were determined using the *ptx-lacZ* (C) or *fha-lacZ* (D) reporter under basal conditions (0) or after the perception of 4 mM chloronicotinate (CN 4). Data shown are means and standard errors of the means.

with Cys or Ala yielded BvgS variants insensitive to nicotinate, i.e., locked in the kinase state (Fig. 6C and D; also Fig. S8A). As expected, S-S bond formation for the latter variants was not significantly modified following the perception of a modulator. The dramatic effects of several substitutions in this region on BvgS function emphasize that the composition of the noncanonical coiled coil is critical for signal transduction.

Effect of modulation on PAS domain quaternary structure. Finally, we determined the effects of modulation on the PAS domain interface. We have shown previously that recombinant PAS proteins of BvgS dimerize (28). Although one can easily model a PAS monomer on the basis of the numerous existing crystallographic structures of PAS domains, it is much more difficult to predict how a given PAS domain of unknown structure dimerizes, since different dimer organizations may occur. Nevertheless, the β-sheet is frequently involved in dimerization and signal transduction (22, 27, 37, 38). We thus performed Cys-scanning analyses targeting the PAS β-sheet (Fig. 7A). At the basal state, all positions allowed low proportions of S-S bond-mediated cross-links (Fig. 7B and C), a finding consistent with a loose dimeric interface or with collision-induced dimerization caused by strong dynamics of the PAS monomers. Instances of low-efficiency cross-linking at successive positions suggest that the PAS domains are plastic and that some substitutions might distort their β-sheets. Of note, shifts in the register of the β-sheet have been reported to contribute to the function of another PAS domain (39). In the modulated state, dimer formation decreased at all positions, indicating a change in the quaternary structure of the PAS domains that might globally correspond to their splaying out (Fig. 7B and C).

The effects of Cys substitutions on the activity of BvgS and its response to modulation were determined (Fig. 7D and E). Most substitutions considerably reduced BvgS kinase activity or abolished it altogether, in particular when hydrophobic residues were replaced, as in $BvgS^{fl}_{Y596C}$, $BvgS^{fl}_{V672C}$, $BvgS^{fl}_{I677C}$, and $BvgS^{fl}_{I689C}$. BvgS was detected at very low levels in *B. pertussis* when Cys was substituted at position 605, 676, 677, or 689, indicating a defect in biogenesis or an increased sensitivity to proteolysis (Fig. S5C in the supplemental material). In addition, the $BvgS^{fl}_{I595C}$, $BvgS^{fl}_{L606C}$, $BvgS^{fl}_{H671C}$, and $BvgS^{fl}_{T676C}$ variants were less sensitive to modulation than $BvgS^{fl}$ (Fig. 7E). The observation that the PAS core domain does not readily tolerate substitutions indicates that its integrity is important for BvgS function, which makes interpretation of the cross-linking results in this region delicate. Nevertheless, dimer formation globally decreased when nicotinate was added to the bacteria, arguing in favor of a change of interface. This change is likely to have a direct effect on the downstream linker 2, whose conformation and dynamics eventually determine the mode of activity of the enzymatic moiety (29).

DISCUSSION

Two-component systems are employed by bacteria in mounting adaptive responses upon the perception of a stimulus. Signal transduction between the perception and the enzymatic domains of sensor kinases generally involves combinations of rotation, scissor, or piston movements of coiled-coil regions (40–49). A simple model is that a sensor kinase populates two thermodynamically stable structural states. Stimulus perception shifts this equilibrium, and the transition of one domain changes the probability for the next domain to shift to the alternative state (46). In BvgS, kinase activity at the basal state is characterized by clamshell motions of the VFT1 domains and by considerable dynamics of linker 2, which precedes the enzymatic moiety (7, 29). Nicotinate binding rigidifies the VFT domains (12). Linker 2 responds to these changes by adopting a stable conformation centered on its hydrophobic coiled-coil interface (29), and the enzymatic module of the protein shifts to phosphatase activity. In this work, we show that signal transmission by the intervening linker 1 in response to modulation involves conformational changes that eventually modify the PAS domain interface. The PAS domains thus appear to amplify small conformational changes of the C-terminal portion of linker 1 to elicit the activity shift.

Our studies suggest the following model for mechanical signal transduction between the periplasmic and enzymatic domains. For the sake of simplicity, we describe two distinct states for BvgS, although it is likely that the kinase and phosphatase modes actually correspond to the coexistence of these two states in different proportions. Under default, kinase-promoting conditions, the short periplasmic cable-like regions of linker 1 follow the VFT dynamics and generate small up-and-down motions of the TM

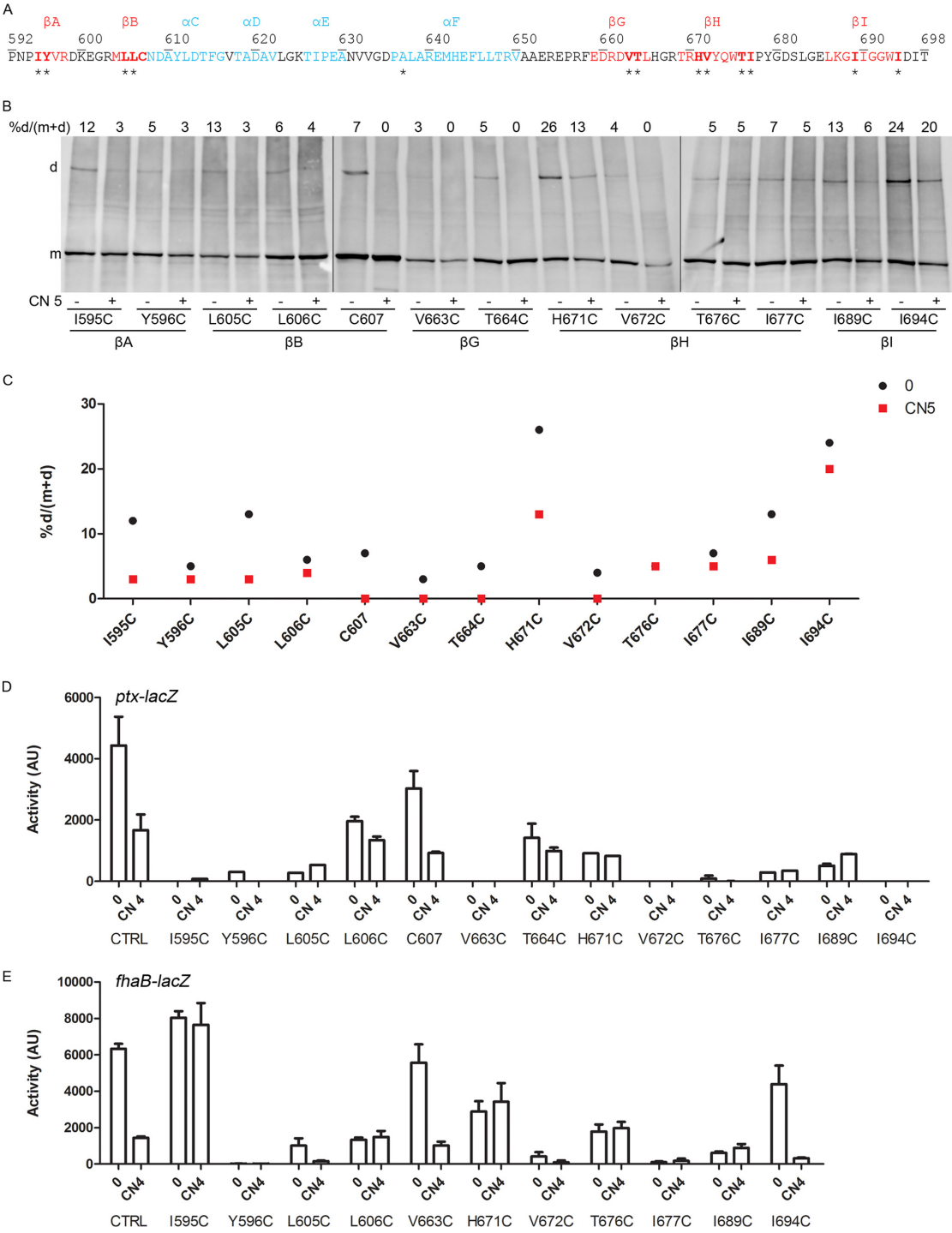

FIG 7 PAS domain organization and effect of modulation. (A) Sequence of the PAS domain with secondary-structure predictions (blue, α-helices; red, β-strands). Residues targeted for Cys scanning are indicated by asterisks. (B) Cys-scanning S-S cross-linking analyses for the BvgS^{t} variants were performed under basal conditions (−) or after the addition (+) of 5 mM chloronicotinate (CN 5). Experimental details are the same as those for Fig. 3. (C) The results of a representative experiment were graphed to facilitate reading. (D and E) The activities of the BvgS^{fl} variants were determined using the *ptx-lacZ* (D) or *fha-lacZ* (E) reporter under basal conditions (0) or after the perception of 4 mM chloronicotinate (CN 4). Data shown are means and standard errors of the means.

segments. The small oscillations of the TM segments are compatible with the coiled-coil conformation of linker 1. This conformation sets the PAS domains in a loosely dimeric state, resulting in a dynamic linker 2, and most likely in a dynamic asymmetry of the DHp helices of the kinase moiety, as described for other systems (50–53). The dynamics

of VFT domains exert some leverage on the membrane surface. Interestingly, the VFT2 domains harbor surface polar or charged residues—Asp_{404}, Lys_{477}, Asp_{413}, Asp_{410}, Asn_{453}, and Gln_{455}—positioned to interact with the head groups of the inner membrane phospholipids (7). Simultaneous replacement of these residues with Ala yielded a variant with markedly decreased kinase activity (E. Lesne, unpublished data), a finding consistent with the model.

In response to modulation, BvgS adopts a distinct state of conformation and dynamics. The decreased dynamics and increased compactness of the periplasmic moiety (12) are transmitted to the PAS domain by small conformational changes of linker 1. This signaling appears to involve a small symmetrical displacement of the TM helices of BvgS toward the periplasm. Piston motions of similar amplitudes are not unprecedented in sensory proteins; asymmetric and symmetric 1- to 2-Å piston motions have been reported for the chemoreceptors Tar and Tsr, as well as for the sensor kinases NarX and TorS, respectively (34, 40, 54, 55).

The penetration of the cytoplasmic portion of linker 1 into the membrane caused by this movement is likely limited by the presence of Arg residues immediately after the hydrophobic region. These residues are conserved in the family and are required for the BvgS response to modulators. They might serve as buoys or anchors to the phospholipid head groups at the cytoplasmic face of the membrane, as in the sensor kinase DesK (56). The TM helices might also accommodate the motion toward the periplasm by stretching, a scenario similar to that proposed for the TM helices of DesK in response to membrane thickening (56). Tension on the TM segment affects the cytoplasmic region of linker 1. Thus, the coiled-coil conformation appears to be disrupted after the conserved residue Q_{580} down to the PAS domain, as shown by the loss of a periodic cross-linking pattern in the C-terminal portion of linker 1. Disruption of the coiled coil upstream affects the PAS domain quaternary structure. This, in turn, enables linker 2 to adopt a stable coiled-coil conformation. The system transitions to the phosphatase mode.

The noncanonical coiled coil in the cytoplasmic portion of linker 1 is necessary for BvgS regulation. Coiled coils involved in signaling have been shown to frequently harbor 1-, 3-, or 4-residue insertions, called skip, stammer, and stutter, respectively, enabling them to transition between distinct conformational states (18). These insertions are accommodated in different ways in the distinct states of activity of sensor kinases (18). In the cytoplasmic portion of linker 1, it is possible to predict two distinct heptad-based coiled-coil registers (Fig. 1B), and the shift of register may correspond to a stutter. The sequence and the results of Cys scanning are also compatible with the adoption of a right-handed, 11-residue coiled-coil conformation by linker 1 (36). In the kinase state, a noncanonical coiled coil—either heptad based with a stutter or hendecad based—is formed, as indicated by a periodic pattern of intermonomer cross-linking. In the phosphatase state, this periodic pattern is disrupted in the C-terminal portion of linker 1, which corresponds to a change in coiled-coil packing, or to the splaying out of the C-terminal portions of the α-helices. Consequently, the PAS domains modify their interface or dissociate.

Small sequence changes in linker 1 hamper signaling, as described in this and earlier work (57–59). Strengthening the C-terminal region of the coiled coil by the replacement of M_{584}, at a central position, with Leu hampers the response to nicotinate, most likely because it disfavors the conformational transition to the phosphatase state. Various spontaneous mutations in this region have been reported previously to yield kinase-locked variants (57–59). Notably, several of those substitutions modify charged residues in noninterfacial coiled-coil positions (e.g., $R_{572}Q$, $R_{575}C$, $D_{579}N$). This suggests that H bonds between side chains within the helices, which probably strengthen them, are necessary for the transition. Taken together, both this study and our previous work show that intermediate levels of coil stability are salient features in BvgS, as expected for a dynamic system that oscillates between distinct states of activity (29).

The role of the PAS domain in BvgS has long remained enigmatic (28). Recently, we have discovered that it may be dispensable for BvgS activity under certain conditions

(29). Thus, some BvgS chimeras in which the PAS domain was replaced with the linkers of PAS-less homologs were functional, especially for long linkers. The present study indicates that the PAS domain serves as a signal amplifier. Thus, a small change of the coiled coil upstream makes the PAS domains splay out, which most likely enables the linker 2 coiled coil underneath to adopt a stable, Leu-zipper-like conformation (29). We speculate that in the kinase-to-phosphatase transition, the connections of the PAS cores with their flanking C-terminal α-helices break. The highly conserved Asp residue of the "DIT" motif, which frequently terminates PAS core domains, mediates interactions of the core with these helices (22, 39–41). In BvgS, replacement of this Asp_{695} residue with Ala abolished kinase activity, a finding consistent with this scenario (28). Conformational changes of the helices flanking the PAS core and modifications of the connections between the PAS core and these helices are frequently involved in signaling in other sensor kinases (26, 60).

The features of linker 1, particularly in its cytoplasmic portion, are rather conserved in the BvgS family. It is thus likely that our findings will be applicable in a general manner to the regulation of homologs. However, 35% of BvgS homologs harboring two VFT domains lack a PAS domain (29). In these proteins, α-helices of variable lengths are predicted to link the VFT and HK domains. This situation would correspond to joining linker 1 and linker 2 to form a single linker. Interestingly, the linkers of the PAS-less sensor kinases show sequence similarity to linkers 1 and 2 of BvgS (29), with key conserved Arg, Gln, and Leu residues. We are currently trying to determine how the mechanism described in this work could be transposed to homologs of BvgS that lack a PAS domain.

MATERIALS AND METHODS

Strains, plasmids, and culture conditions. *B. pertussis* was first grown on Bordet-Gengou agar plates for 2 days at 37°C and then cultured in modified Stainer-Scholte (SS) liquid medium at 37°C under agitation. All the $BvgS^{fl}$ variants were constructed by mutagenesis and cassette exchange in the pBBRmpla plasmid (7). However, for the $BvgS_{R564A}$, $BvgS_{R564A\text{-}R565A}$, and $BvgS_{R564A\text{-}R565A\text{-}R568A}$ variants, mutagenesis fragments were cloned first into the intermediate plasmid pUC19mos and then into pSS1129, in order to be introduced by allelic exchange into the chromosome of *B. pertussis* $BPSM_{\Delta}$bvgAS as in references 7 and 14. To construct the variants with modified linker lengths, synthetic gene portions (GeneCust, Luxembourg) were introduced by BglII-XbaI cassette exchange into pUC19mpla to replace the wild-type (wt) fragment before the transfer of the EcoRI-HindIII fragment of the resulting plasmid into the mobilizable pBBR1-MCS4 plasmid, yielding pBBRmpla variants (7).

The recombinant *B. pertussis* strains were produced by introducing the plasmid variants by conjugation into *B. pertussis* $BPSM_{new\Delta}$AS carrying the chromosomal *ptx-lacZ* or *fhaB-lacZ* transcriptional fusion (7). The transcriptional fusions used as reporters have been described previously (61). The $BvgS^{t}$ variants used for Cys-scanning analyses in *E. coli* were based on the pPORVPH plasmid (29). They were constructed by mutagenesis followed by cassette exchanges as described previously (29).

Protein sequence analyses. The search for putative sensor kinases of the BvgS family was performed as described previously (29) on the NR database (release of 16 November 2016; 73,037,689 sequences) from the National Center for Biotechnology Information (NCBI). Using a customized Python script, we selected the sequences containing two VFT domains and a kinase domain, which resulted in 6,330 proteins. A modified version of this script was used to retain only the sequences containing PAS domains by selecting for the presence of at least 200 residues between the end of the VFT domain and the His residue of the kinase. This yielded 4,377 sequences, from which we selected those predicted to harbor a single PAS domain by retaining predicted proteins with 217 to 265 residues between the end of the VFT domain and the His residue of the kinase. This selection yielded 3,988 sequences. We then used CD-HIT (62) to reduce the sequence redundancy of the resulting data set so as to ensure that the sequence identity of any two sequences was no more than 90%. This resulted in 577 sequences, of which 16 were discarded because they appeared to lack a predicted TM domain.

The sequences were aligned with ClustalW (63), and the alignments were edited using Jalview (64). These alignments were illustrated by a logo representation using WebLogo (65). The alignments were also used with BioPython to generate the matrices shown in the supplemental material.

Cys-scanning analyses. Cys-scanning analyses were performed in *E. coli* UT5600 carrying the pPORVPH variants as in reference 29. Modifications to this protocol were introduced to enhance cross-linking in the hydrophobic environment of the membrane. Thus, the bacteria that produce $BvgS^{t}$ with a Cys residue in the predicted TM segment were cultured in filtered LB medium (LB broth [Lennox]; Difco), and an oxidative treatment was carried out in the same culture medium by using 1 mM copper-*o*-phenanthroline for 20 min. The rest of the experimental protocol was the same as that described previously (29). The Cys-scanning analyses were performed at least twice for each position, and the results were reproducible.

Cys accessibility. Cys accessibility analyses were performed on BvgS^{fl} Cys variants. We first checked that the three Cys residues present in the receiver and HPt domains were blocked by the *N*-ethylmaleimide (NEM; Sigma) treatment and thus were not labeled with PEG-maleimide (Peg-Mal, 20 kDa; tebu-bio or Sigma). *B. pertussis* carrying plasmids with each of the BvgS^{fl} Cys variants was grown in 10 ml of SS medium for 24 h at 37°C, with rotary shaking at 200 rpm. Where indicated, 4 mM chloronicotinate was added to the culture medium for 30 min before culture centrifugation for 15 min at 9,000 × *g* and 37°C. Cell pellets were washed with 50 mM sodium phosphate, pH 6.8 (NaP), supplemented or not with chloronicotinate (4 mM). After centrifugation, the pellets were suspended in 2 ml of NaP supplemented with protease inhibitors (Complete EDTA-free [Roche]; 1 tablet per 50 ml of buffer), 4 mM chloronicotinate where indicated, and 5 mM NEM, and the suspensions were incubated for 1 h at 37°C without shaking. After centrifugation to harvest the cells, the pellets were first washed twice in NaP and then resuspended at an optical density at 600 nm (OD_{600}) of 5 per ml in this buffer supplemented with protease inhibitors and 10 μg/ml DNase I. The bacteria were lysed using a Hybaid Ribolyser apparatus (for 50 s at speed 6), and membrane proteins were harvested from the clarified lysates by ultracentrifugation at 90,000 × *g* for 1 h at 8°C. The pellets were resuspended in 64 μl NaP, and 16 μl of 10% SDS was added before incubation of the samples for 1 h at 37°C with slow shaking. The nonmodified Cys side chains were labeled by adding 1 mM Peg-Mal to the samples and incubating for 1 h at 37°C without shaking. Loading buffer (33.3 μl NuPAGE lithium dodecyl sulfate [LDS] sample buffer [4×]; Life Technologies) was added before the sample was heated at 70°C for 10 min. The proteins were then separated by electrophoresis using 3 to 8% Tris-acetate gels (NuPAGE Novex; Life Technologies). Immunoblot analyses were performed as described previously, except that the primary antibodies against BvgS (28) were used at a 1:2,000 dilution. The secondary antibodies (horseradish peroxidase [HRP]-conjugated anti-rat antibodies; Abcam) were diluted to 1:10,000. Following immunoblot analysis using the Amersham ECL Prime Western blot detection system (GE Healthcare) and an Amersham Imager 600 (GE Healthcare), band intensities were quantified using ImageQuant TL software. The Cys accessibility experiments were performed at least twice for each position at the junction between the hydrophobic and polar layers of the membrane, and the results were reproducible. One experiment was performed for the solvent-accessible positions.

Other methods. β-Galactosidase assays were performed as described previously (7) with three different clones at different times, and the means and standard errors of the means were determined. For the detection of inactive BvgS variants in *B. pertussis*, the bacteria were lysed, and the membrane proteins were harvested by ultracentrifugation as described above. For the Cys variants, 10 mM NEM was added to the resuspended pellet before lysis to avoid S-S bond formation during sample handling. Electrophoresis and immunoblotting were performed as described above.

SUPPLEMENTAL MATERIAL

Supplemental material for this article may be found at https://doi.org/10.1128/JB.00114-17.

SUPPLEMENTAL FILE 1, PDF file, 4.8 MB.

ACKNOWLEDGMENTS

F.J.-D. and R.A. designed the project; E.L. conceived and performed the experiments; F.J.-D., E.L., E.D., and R.A analyzed the data; E.L., C.L., and F.J.-D. wrote the paper; and all authors edited it.

We thank Mariem Ben Aissa and Emmanuelle Petit for help with mutant construction.

This work was funded by grant ANR-13-BSV8-0002-01 to F.J.-D. E.L. received a doctoral fellowship from the Region Nord Pas de Calais and INSERM.

The funders had no role in study design, data collection and interpretation, or the decision to submit the work for publication.

REFERENCES

1. Beier D, Gross R. 2006. Regulation of bacterial virulence by two-component systems. Curr Opin Microbiol 9:143–152. https://doi.org/10.1016/j.mib.2006.01.005.
2. Bekker M, Teixeira de Mattos MJ, Hellingwerf KJ. 2006. The role of two-component regulation systems in the physiology of the bacterial cell. Sci Prog 89:213–242. https://doi.org/10.3184/003685006783238308.
3. Stock AM, Robinson VL, Goudreau PN. 2000. Two-component signal transduction. Annu Rev Biochem 69:183–215. https://doi.org/10.1146/annurev.biochem.69.1.183.
4. Zschiedrich CP, Keidel V, Szurmant H. 2016. Molecular mechanisms of two-component signal transduction. J Mol Biol 428:3752–3775. https://doi.org/10.1016/j.jmb.2016.08.003.
5. Gao R, Stock AM. 2009. Biological insights from structures of two-component proteins. Annu Rev Microbiol 63:133–154. https://doi.org/10.1146/annurev.micro.091208.073214.
6. Cotter PA, Jones AM. 2003. Phosphorelay control of virulence gene expression in *Bordetella*. Trends Microbiol 11:367–373. https://doi.org/10.1016/S0966-842X(03)00156-2.
7. Dupré E, Herrou J, Lensink MF, Wintjens R, Vagin A, Lebedev A, Crosson S, Villeret V, Locht C, Antoine R, Jacob-Dubuisson F. 2015. Virulence regulation with Venus flytrap domains: structure and function of the periplasmic moiety of the sensor-kinase BvgS. PLoS Pathog 11:e1004700. https://doi.org/10.1371/journal.ppat.1004700.
8. Hoch JA. 2000. Two-component and phosphorelay signal transduction. Curr Opin Microbiol 2:165–170. https://doi.org/10.1016/S1369-5274(00)00070-9.

9. Lacey BW. 1960. Antigenic modulation of *Bordetella pertussis*. J Hyg (Lond) 31:423–434.
10. Melton AR, Weiss AA. 1993. Characterization of environmental regulators of *Bordetella pertussis*. Infect Immun 61:807–815.
11. Nakamura MM, Liew SY, Cummings CA, Brinig MM, Dieterich C, Relman DA. 2006. Growth phase- and nutrient limitation-associated transcript abundance regulation in *Bordetella pertussis*. Infect Immun 74:5537–5548. https://doi.org/10.1128/IAI.00781-06.
12. Dupré E, Lesne E, Guerin J, Lensink MF, Verger A, de Ruyck J, Brysbaert G, Vezin H, Locht C, Antoine R, Jacob-Dubuisson F. 2015. Signal transduction by BvgS sensor-kinase binding of modulator nicotinate affects conformation and dynamics of entire periplasmic moiety. J Biol Chem 290:23307–23319. https://doi.org/10.1074/jbc.M115.655720.
13. Herrou J, Bompard C, Wintjens R, Dupré E, Willery E, Villeret V, Locht C, Antoine R, Jacob-Dubuisson F. 2010. Periplasmic domain of the sensor-kinase BvgS reveals a new paradigm for the Venus flytrap mechanism. Proc Natl Acad Sci U S A 107:17351–17355. https://doi.org/10.1073/pnas.1006267107.
14. Herrou J, Debrie AS, Willery E, Renaud-Mongenie G, Locht C, Mooi F, Jacob-Dubuisson F, Antoine R. 2009. Molecular evolution of the two-component system BvgAS involved in virulence regulation in *Bordetella*. PLoS One 4:e6996. https://doi.org/10.1371/journal.pone.0006996.
15. Jacob-Dubuisson F, Wintjens R, Herrou J, Dupré E, Antoine R. 2012. BvgS of pathogenic bordetellae: a paradigm for sensor-kinases with Venus flytrap perception domains, p 57–83. *In* Gross R, Beier D (ed), Two-component systems in bacteria. Caister Academic Press, Norfolk, United Kingdom.
16. Gruber M, Soding J, Lupas AN. 2006. Comparative analysis of coiled-coil prediction methods. J Struct Biol 155:140–145. https://doi.org/10.1016/j.jsb.2006.03.009.
17. Woolfson DN. 2005. The design of coiled-coil structures and assemblies. Adv Protein Chem 70:79–112. https://doi.org/10.1016/S0065-3233(05)70004-8.
18. Schmidt NW, Grigoryan G, DeGrado WF. 2017. The accommodation index measures the perturbation associated with insertions and deletions in coiled-coils: application to understand signaling in histidine kinases. Protein Sci 26:414–435. https://doi.org/10.1002/pro.3095.
19. Mason JM, Arndt KM. 2004. Coiled coil domains: stability, specificity, and biological implications. Chembiochem 5:170–176. https://doi.org/10.1002/cbic.200300781.
20. Grigoryan G, Keating AE. 2008. Structural specificity in coiled-coil interactions. Curr Opin Struct Biol 18:477–483. https://doi.org/10.1016/j.sbi.2008.04.008.
21. Meier M, Stetefeld J, Burkhard P. 2010. The many types of interhelical ionic interactions in coiled coils—an overview. J Struct Biol 170:192–201. https://doi.org/10.1016/j.jsb.2010.03.003.
22. Möglich A, Ayers RA, Moffat K. 2009. Structure and signaling mechanism of Per-ARNT-Sim domains. Structure 17:1282–1294. https://doi.org/10.1016/j.str.2009.08.011.
23. Henry JT, Crosson S. 2011. Ligand-binding PAS domains in a genomic, cellular, and structural context. Annu Rev Microbiol 65:261–286. https://doi.org/10.1146/annurev-micro-121809-151631.
24. Taylor BL, Zhulin IB. 1999. PAS domains: internal sensors of oxygen, redox potential, and light. Microbiol Mol Biol Rev 63:479–506.
25. Ayers RA, Moffat K. 2008. Changes in quaternary structure in the signaling mechanisms of PAS domains. Biochemistry 47:12078–12086. https://doi.org/10.1021/bi801254c.
26. Key J, Hefti M, Purcell EB, Moffat K. 2007. Structure of the redox sensor domain of *Azotobacter vinelandii* NifL at atomic resolution: signaling, dimerization, and mechanism. Biochemistry 46:3614–3623. https://doi.org/10.1021/bi0620407.
27. Herrou J, Crosson S. 2011. Function, structure and mechanism of bacterial photosensory LOV proteins. Nat Rev Microbiol 9:713–723. https://doi.org/10.1038/nrmicro2622.
28. Dupré E, Wohlkonig A, Herrou J, Locht C, Jacob-Dubuisson F, Antoine R. 2013. Characterization of the PAS domain in the sensor-kinase BvgS: mechanical role in signal transmission. BMC Microbiol 13:172. https://doi.org/10.1186/1471-2180-13-172.
29. Lesne E, Krammer EM, Dupré E, Locht C, Lensink MF, Antoine R, Jacob-Dubuisson F. 2016. Balance between coiled-coil stability and dynamics regulates activity of BvgS sensor kinase in *Bordetella*. mBio 7:e02089. https://doi.org/10.1128/mBio.02089-15.
30. Parry DA, Fraser RD, Squire JM. 2008. Fifty years of coiled-coils and alpha-helical bundles: a close relationship between sequence and structure. J Struct Biol 163:258–269. https://doi.org/10.1016/j.jsb.2008.01.016.
31. Lupas AN, Gruber M. 2005. The structure of alpha-helical coiled coils. Adv Protein Chem 70:37–78. https://doi.org/10.1016/S0065-3233(05)70003-6.
32. Jones AM, Boucher PE, Williams CL, Stibitz S, Cotter PA. 2005. Role of BvgA phosphorylation and DNA binding affinity in control of Bvg-mediated phenotypic phase transition in *Bordetella pertussis*. Mol Microbiol 58:700–713. https://doi.org/10.1111/j.1365-2958.2005.04875.x.
33. Bass RB, Butler SL, Chervitz SA, Gloor SL, Falke JJ. 2007. Use of site-directed cysteine and disulfide chemistry to probe protein structure and dynamics: applications to soluble and transmembrane receptors of bacterial chemotaxis. Methods Enzymol 423:25–51. https://doi.org/10.1016/S0076-6879(07)23002-2.
34. Monzel C, Unden G. 2015. Transmembrane signaling in the sensor kinase DcuS of *Escherichia coli*: a long-range piston-type displacement of transmembrane helix 2. Proc Natl Acad Sci U S A 112:11042–11047. https://doi.org/10.1073/pnas.1507217112.
35. Heininger A, Yusuf R, Lawrence RJ, Draheim RR. 2016. Identification of transmembrane helix 1 (TM1) surfaces important for EnvZ dimerisation and signal output. Biochim Biophys Acta 1858:1868–1875. https://doi.org/10.1016/j.bbamem.2016.05.002.
36. Gruber M, Lupas AN. 2003. Historical review: another 50th anniversary—new periodicities in coiled coils. Trends Biochem Sci 28:679–685. https://doi.org/10.1016/j.tibs.2003.10.008.
37. Little R, Salinas P, Slavny P, Clarke TA, Dixon R. 2011. Substitutions in the redox-sensing PAS domain of the NifL regulatory protein define an inter-subunit pathway for redox signal transmission. Mol Microbiol 82:222–235. https://doi.org/10.1111/j.1365-2958.2011.07812.x.
38. Slavny P, Little R, Salinas P, Clarke TA, Dixon R. 2010. Quaternary structure changes in a second Per-Arnt-Sim domain mediate intramolecular redox signal relay in the NifL regulatory protein. Mol Microbiol 75:61–75. https://doi.org/10.1111/j.1365-2958.2009.06956.x.
39. Evans MR, Card PB, Gardner KH. 2009. ARNT PAS-B has a fragile native state structure with an alternative beta-sheet register nearby in sequence space. Proc Natl Acad Sci U S A 106:2617–2622. https://doi.org/10.1073/pnas.0808270106.
40. Bhate MP, Molnar KS, Goulian M, DeGrado WF. 2015. Signal transduction in histidine kinases: insights from new structures. Structure 23:981–994. https://doi.org/10.1016/j.str.2015.04.002.
41. Möglich A, Ayers RA, Moffat K. 2009. Design and signaling mechanism of light-regulated histidine kinases. J Mol Biol 385:1433–1444. https://doi.org/10.1016/j.jmb.2008.12.017.
42. Ferris HU, Dunin-Horkawicz S, Hornig N, Hulko M, Martin J, Schultz JE, Zeth K, Lupas AN, Coles M. 2012. Mechanism of regulation of receptor histidine kinases. Structure 20:56–66. https://doi.org/10.1016/j.str.2011.11.014.
43. Hulko M, Berndt F, Gruber M, Linder JU, Truffault V, Schultz A, Martin J, Schultz JE, Lupas AN, Coles M. 2006. The HAMP domain structure implies helix rotation in transmembrane signaling. Cell 126:929–940. https://doi.org/10.1016/j.cell.2006.06.058.
44. Lemmin T, Soto CS, Clinthorne G, DeGrado WF, Dal Peraro M. 2013. Assembly of the transmembrane domain of *E. coli* PhoQ histidine kinase: implications for signal transduction from molecular simulations. PLoS Comput Biol 9:e1002878. https://doi.org/10.1371/journal.pcbi.1002878.
45. Matamouros S, Hager KR, Miller SI. 2015. HAMP domain rotation and tilting movements associated with signal transduction in the PhoQ sensor kinase. mBio 6:e00616-15. https://doi.org/10.1128/mBio.00616-15.
46. Molnar KS, Bonomi M, Pellarin R, Clinthorne GD, Gonzalez G, Goldberg SD, Goulian M, Sali A, DeGrado WF. 2014. Cys-scanning disulfide crosslinking and Bayesian modeling probe the transmembrane signaling mechanism of the histidine kinase, PhoQ. Structure 22:1239–1251. https://doi.org/10.1016/j.str.2014.04.019.
47. Falke JJ, Hazelbauer GL. 2001. Transmembrane signaling in bacterial chemoreceptors. Trends Biochem Sci 26:257–265. https://doi.org/10.1016/S0968-0004(00)01770-9.
48. Diensthuber RP, Bommer M, Gleichmann T, Möglich A. 2013. Full-length structure of a sensor histidine kinase pinpoints coaxial coiled coils as signal transducers and modulators. Structure 21:1127–1136. https://doi.org/10.1016/j.str.2013.04.024.
49. Lowe EC, Basle A, Czjzek M, Firbank SJ, Bolam DN. 2012. A scissor blade-like closing mechanism implicated in transmembrane signaling in a *Bacteroides* hybrid two-component system. Proc Natl Acad Sci U S A 109:7298–7303. https://doi.org/10.1073/pnas.1200479109.

50. Ferris HU, Coles M, Lupas AN, Hartmann MD. 2014. Crystallographic snapshot of the *Escherichia coli* EnvZ histidine kinase in an active conformation. J Struct Biol 186:376–379. https://doi.org/10.1016/j.jsb.2014.03.014.
51. Mechaly AE, Sassoon N, Betton JM, Alzari PM. 2014. Segmental helical motions and dynamical asymmetry modulate histidine kinase autophosphorylation. PLoS Biol 12:e1001776. https://doi.org/10.1371/journal.pbio.1001776.
52. Wang C, Sang J, Wang J, Su M, Downey JS, Wu Q, Wang S, Cai Y, Xu X, Wu J, Senadheera DB, Cvitkovitch DG, Chen L, Goodman SD, Han A. 2013. Mechanistic insights revealed by the crystal structure of a histidine kinase with signal transducer and sensor domains. PLoS Biol 11:e1001493. https://doi.org/10.1371/journal.pbio.1001493.
53. Trajtenberg F, Imelio JA, Machado MR, Larrieux N, Marti MA, Obal G, Mechaly AE, Buschiazzo A. 2016. Regulation of signaling directionality revealed by 3D snapshots of a kinase:regulator complex in action. eLife 5:e21422. https://doi.org/10.7554/eLife.21422.
54. Moore JO, Hendrickson WA. 2009. Structural analysis of sensor domains from the TMAO-responsive histidine kinase receptor TorS. Structure 17:1195–1204. https://doi.org/10.1016/j.str.2009.07.015.
55. Hazelbauer GL, Falke JJ, Parkinson JS. 2008. Bacterial chemoreceptors: high-performance signaling in networked arrays. Trends Biochem Sci 33:9–19. https://doi.org/10.1016/j.tibs.2007.09.014.
56. Saita E, Abriata LA, Tsai YT, Trajtenberg F, Lemmin T, Buschiazzo A, Dal Peraro M, de Mendoza D, Albanesi D. 2015. A coiled coil switch mediates cold sensing by the thermosensory protein DesK. Mol Microbiol 98:258–271. https://doi.org/10.1111/mmi.13118.
57. Miller JF, Johnson SA, Black WJ, Beattie DT, Mekalanos JJ, Falkow S. 1992. Constitutive sensory transduction mutations in the *Bordetella pertussis bvgS* gene. J Bacteriol 174:970–979. https://doi.org/10.1128/jb.174.3.970-979.1992.
58. Goyard S, Bellalou J, Mireau H, Ullmann A. 1994. Mutations in the *Bordetella pertussis bvgS* gene that confer altered expression of the *fhaB* gene in *Escherichia coli*. J Bacteriol 176:5163–5166. https://doi.org/10.1128/jb.176.16.5163-5166.1994.
59. Manetti R, Arico B, Rappuoli R, Scarlato V. 1994. Mutations in the linker region of BvgS abolish response to environmental signals for the regulation of the virulence factors in *Bordetella pertussis*. Gene 150:123–127. https://doi.org/10.1016/0378-1119(94)90870-2.
60. Philip AF, Kumauchi M, Hoff WD. 2010. Robustness and evolvability in the functional anatomy of a PER-ARNT-SIM (PAS) domain. Proc Natl Acad Sci U S A 107:17986–17991. https://doi.org/10.1073/pnas.1004823107.
61. Antoine R, Alonso S, Raze D, Coutte L, Lesjean S, Willery E, Locht C, Jacob-Dubuisson F. 2000. New virulence-activated and virulence-repressed genes identified by systematic gene inactivation and generation of transcriptional fusions in *Bordetella pertussis*. J Bacteriol 182:5902–5905. https://doi.org/10.1128/JB.182.20.5902-5905.2000.
62. Li W, Godzik A. 2006. Cd-hit: a fast program for clustering and comparing large sets of protein or nucleotide sequences. Bioinformatics 22:1658–1659. https://doi.org/10.1093/bioinformatics/btl158.
63. Larkin MA, Blackshields G, Brown NP, Chenna R, McGettigan PA, McWilliam H, Valentin F, Wallace IM, Wilm A, Lopez R, Thompson JD, Gibson TJ, Higgins DG. 2007. Clustal W and Clustal X version 2.0. Bioinformatics 23:2947–2948. https://doi.org/10.1093/bioinformatics/btm404.
64. Waterhouse A, Procter J, Martin D, Clamp M, Barton G. 2009. Jalview version 2—a multiple sequence alignment editor and analysis workbench. Bioinformatics 25:1189–1191. https://doi.org/10.1093/bioinformatics/btp033.
65. Crooks GE, Hon G, Chandonia JM, Brenner SE. 2004. WebLogo: a sequence logo generator. Genome Res 14:1188–1190. https://doi.org/10.1101/gr.849004.